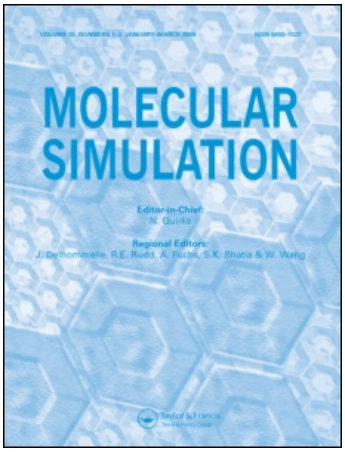

Molecular Simulation
Publication details, including instructions for authors and subscription information:
http://www.informaworld.com/smpp/title~content=t713644482

Molecular modelling studies of calcium carbonate and its nanoparticles

C. A. Bearchell[a]; D. M. Heyes[a]
[a] Department of Chemistry, School of Physics and Chemistry, University of Surrey, Guildford, UK

Online publication date: 26 October 2010

To cite this Article Bearchell, C. A. and Heyes, D. M.(2002) 'Molecular modelling studies of calcium carbonate and its nanoparticles', Molecular Simulation, 28: 6, 517 — 538
To link to this Article: DOI: 10.1080/08927020290030116
URL: http://dx.doi.org/10.1080/08927020290030116

Molecular Simulation, 2002 VOL. 28 (6-7), pp. 517–538

MOLECULAR MODELLING STUDIES OF CALCIUM CARBONATE AND ITS NANOPARTICLES

C.A. BEARCHELL and D.M. HEYES*

Department of Chemistry, School of Physics and Chemistry, University of Surrey, Guildford GU2 7XH, UK

(Received 1 April 2001; In final form 1 August 2001)

Molecular dynamics (MD), simulations have been carried out of crystalline aragonite and calcite, and of finely dispersed calcium carbonate in the form of nanosized inorganic core- organic shell particles. The latter, called overbased detergents commercially, are used as acid-consuming components in automotive and marine engine oils. We have modelled several types of these particles using different surfactant types. We compare the internal structure of the calcium carbonate in these particles with calcite and aragonite crystalline forms using MD in each case. The atomic force-field adopted accounts reasonably well for the crystalline phases, although under unconstrained (constant stress) conditions some distortion of the aragonite structure was noticed. The microstructure of the nanoparticles appears to be quite different to the crystals, and seemingly amorphous. For these small clusters it appears that there is probably no thermodynamic benefit in forming local crystalline order in the cores. The relatively large surface to volume ratio found in these particles lends itself to a more amorphous microstructure.

Keywords: Aragonite; Calcite; Nanoparticles

INTRODUCTION

Calcium carbonate occurs naturally in many forms, in the bulk, as aragonite, calcite and also in a variety of other unusual forms, produced principally by living

*Corresponding author. E-mail: d.heyes@surrey.ac.uk

ISSN 0892-7022 © 2002 Taylor & Francis Ltd
DOI: 10.1080/08927020290030116

organisms [1]. In the latter case these can consist of metastable low dimensional networks or as thermodynamically stable isolated nanoparticles in which the inorganic material forms the inner region of a core-shell particle. The outer surface is coated by an organic surfactant layer. In fact, such core-shell particles are made commercially for dispersal in engine oil as anti-acid additives. These are known, for historical reasons, as overbased detergents, ODs [2–7]. Many different types of surfactant are used commercially in the manufacture of ODs. These include alkyl sulphonates, sulphurised alkyl phenates, salicylates and calixarates [6]. Presumably this is not an exclusive list, and many other surfactant classes would also produce the core-shell arrangements. The neutralising strength of an OD is denoted by the commercial specification "total base number" or TBN for short. The TBN is the acid neutralising ability of one gram of the powdered compound, measured as the number of equivalent mg of KOH that would have the same effect. This value can rise to ca. 500 for some of the newer manufactured products. The value of the TBN scale is that it quantifies the practical usefulness of the product as an anti-acid additive in an objective way across the range, and independent of specific chemical compositions [2].

In this report the results of simulations of the bulk calcium carbonate are presented, and these are compared with OD particles. Some results from our earlier modelling studies have been published elsewhere [2–6] and here we focus on a new aspect of the model calcium carbonate, that is, a comparison between bulk crystalline calcium carbonate ion assembly and that in the nanoparticles. We report the results of molecular dynamics (MD) simulations of bulk calcium carbonate and the nanoparticles. MD simulations have been carried out before to study the properties of molten alkali carbonates [8–10]. These calculations used pair potentials obtained in part from *ab initio* calculations, and gave satisfactory agreement with the experimental microstructures and dynamics. A MD study of molten $CaCO_3$ has also been carried out at pressures and temperatures beyond those accessible to experimental techniques [11]. In this study, two crystalline forms of $CaCO_3$, calcite and aragonite, were modelled and the structures compared with the predictions of X-ray diffraction.

THE MODEL

We have performed constant volume and constant stress simulations of the calcite and aragonite phases of $CaCO_3$ using the force-field of Dove *et al*. [12], which includes bond stretching and bending terms, and an out-of-plane pseudo-potential to maintain planarity of the carbonate anion. For the non-bonded interactions, Coulomb interactions were included between the charged surfactant head groups

and the $CaCO_3$ core ions. The model $CaCO_3$ carbonate charges are given in Table I. The short-range repulsive interactions were represented by the Born–Mayer potential,

$$U_{\text{rep}}(r_{ij}) = A\exp(-r_{ij}/B) \tag{1}$$

with the parameters given in Table II. The intramolecular terms used to describe the carbonate ions had bond-stretching, bond-bending and out-of-plane deformation-resistance potentials. The bond stretching interaction energy was represented using a quadratic function of bond length,

$$U_{\text{stretch}} = \sum_{i=1}^{N_{\text{stretch}}} k_{\text{b}}(r - r_0)^2 \tag{2}$$

where k_{b} is the bond stretching force constant, r_0 the equilibrium bond length, r the interatomic separation [see Fig. 1(a)] and N_{stretch} is the number of participating bonds. The bond-bending terms were implemented using by the following intramolecular potential,

$$U_{\text{bend}} = \sum_{i=1}^{N_{\text{bend}}} k_\theta(\theta - \theta_0)^2 \tag{3}$$

where k_θ is the bond bending force constant, θ_0 is the equilibrium bond angle and θ is the bond angle between the three atoms [see Fig. 1(b)]. The out-of-plane potential, used to keep the carbonate anions flat has the same analytic form as an alkane chain dihedral potential, with the out-of-plane angle taking the form of a dihedral angle interaction between the four carbonate atoms defining the plane. The central carbon atom was taken to be one of the terminal atoms defining the dihedral angle [see Fig. 1(c)]. The potential was then implemented as for the dihedral term with the out-of-plane angle taken as the dihedral angle,

$$U_{\text{out-of-plane}} = \sum_{i=1}^{N_{\text{out-of-plane}}} k_\chi\big(1 + \cos\big((n\chi) - \chi_0\big)\big) \tag{4}$$

where k_x is the out-of-plane force constant, n the periodicity, χ_0 the equilibrium

TABLE I Atomic charges used for simulation of $CaCO_3$ [12]

Atom	Charge (e)
Ca	+1.64203
O	−0.894293
C	+1.04085

TABLE II The Born–Mayer repulsive potential parameters used for the $CaCO_3$ simulations [12]

Interaction	A (eV)	B (Å)
Ca–O	3943.5977	0.251570
O–O	2879.1262	0.252525
C–O	1.7411309×10^{13}	0.03873

out of plane angle (= 0 here) and χ the calculated out of plane angle. The potential parameters for this force-field are given in Table III.

The starting ion co-ordinates in the calcite and aragonite simulations were taken from crystallographic data. Calcite has a rhombohedral crystal structure with the $R\bar{3}c$ spacegroup. The lattice parameters are, $a = b = 4.990$ Å, $c = 17.061$ Å, $\alpha = \beta = 90°$ and $\gamma = 120°$[13]. Aragonite has an orthorhombic crystal structure with the *Pmcn* space group and the lattice parameters are, $a = 4.960$ Å, $b = 7.964$ Å, $c = 5.738$ Å and $\alpha = \beta = \gamma = 90°$ [14]. The calcite simulation cell was composed of 20 unit cells, four unit cells along the *a*axis, five along *b* and one along *c*, while the aragonite simulation cell included 27 unit cells, three along each of the *a*, *b* and *c* axes. Figs. 2 and 3 show the initial calcite

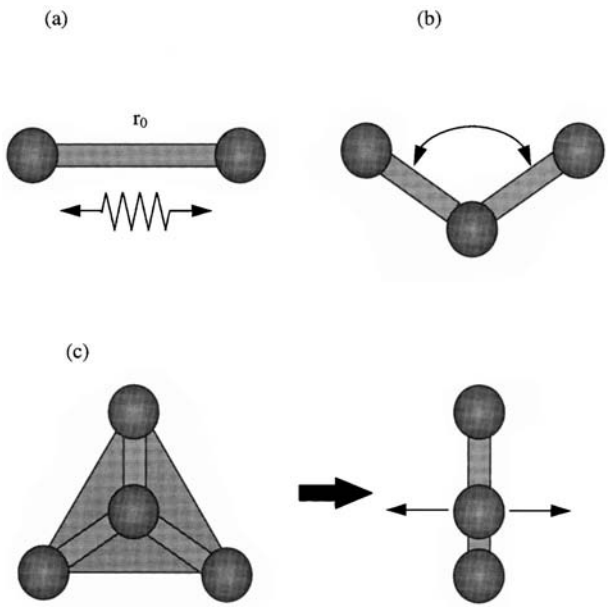

FIGURE 1 (a) The bond stretching term of the carbonate force-field, (b) bond angle term, where r_b and θ_0 are the equilibrium bond length and bond angles, respectively; (c) represents the out-of-plane restraining intramolecular potential.

TABLE III Table of parameters describing the intramolecular interactions of the carbonate ions [12]

Parameter	Value
C–O stretching force constant, k_b	156.8 kJ mol^{-1}
C–O equilibrium bond length, r_0	1.283Å
O–C–O bond bending force constant, k_θ	29.2 kJ mol^{-1}
O–C–O equilibrium bond angle, θ_0	120.0°
Out-of-plane force constant, k_χ	2.4 kJ mol^{-1}
Periodicity of out-of-plane potential, n	2.0
Equilibrium out-of-plane angle, χ_0	180.0°

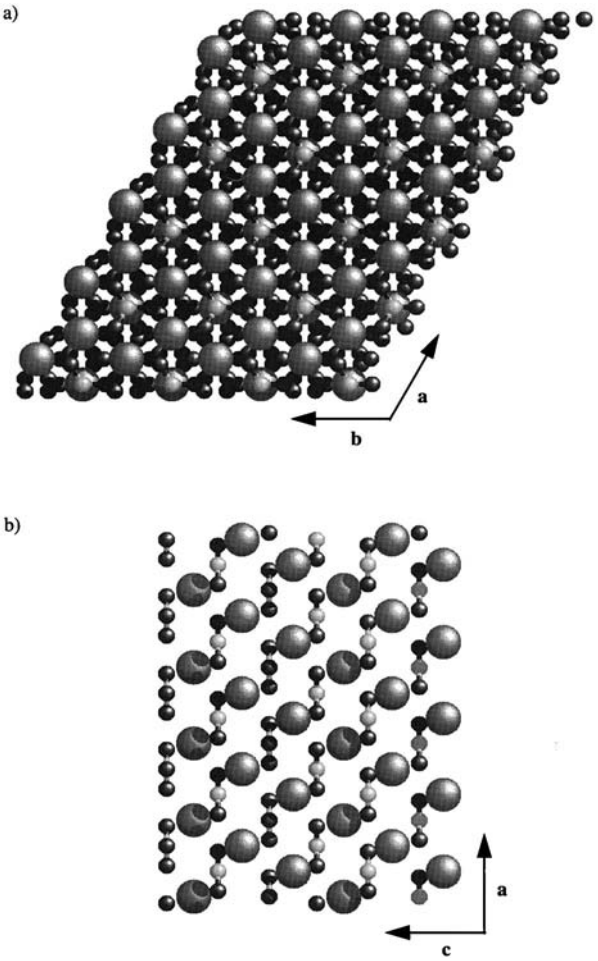

FIGURE 2 The initial starting configuration of the simulation cell for calcite, showing oxygen atoms carbons and calciums. Carbonate ions are shown with a stick representation for the bonds between carbon and oxygen atoms. Key: (a) is the projection along the *c* axis, and (b) is the projection along the *b* axis.

and aragonite systems lattices. Fig. 2(a) shows the calcite simulation cell projected along the *c* axis, and (b) gives a projection along the *b* axis. The aragonite simulation cell in Fig. 3(a) and (b) shows projections along the *c* and *a* axes, respectively.

Two types of simulation where carried out. A constant volume simulation was equilibrated for 500 ps using a timestep of 1.0 fs. A constant stress simulation was then performed at 1 bar hydrostatic pressure and constant temperature of 298 K. The Ewald summation technique was used to calculate the Coulombic

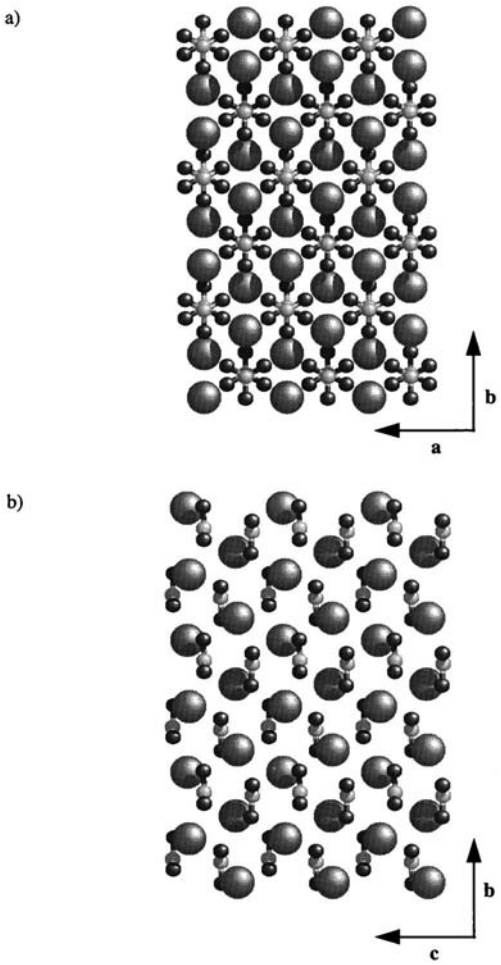

FIGURE 3 The initial starting configuration of the simulation cell for aragonite: (a) and (b) show projections along the *c* and *a* axes, respectively.

contributions to the potential, forces and stress, taking a value of $\kappa = 4.0/L$, where L is the shortest orthogonal cell dimension, for the inverse decay length [15]. Properties were then calculated over a time interval of 200 ps, taking a timestep of 0.5 fs.

Figs. 4 and 5 show the final system configurations of the calcite and aragonite simulations, respectively. Comparison with Fig. 2, for the calcite case, shows there is little difference between the initial and final structures, apart from some thermally induced positional and rotational disorder. For

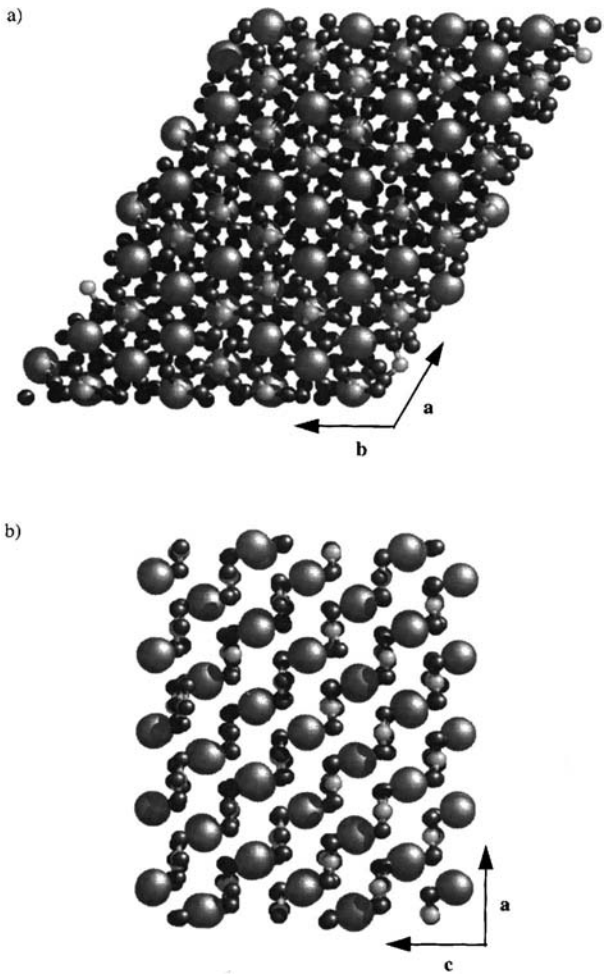

FIGURE 4 The final configuration of a constant volume simulation for calcite: (a) and (b) denote projections along the *c* and *b* axes, respectively. The simulation was carried out at 298 K and a density of 2.71 g cm^{-3}. Other details are as for Figs. 2 and 3.

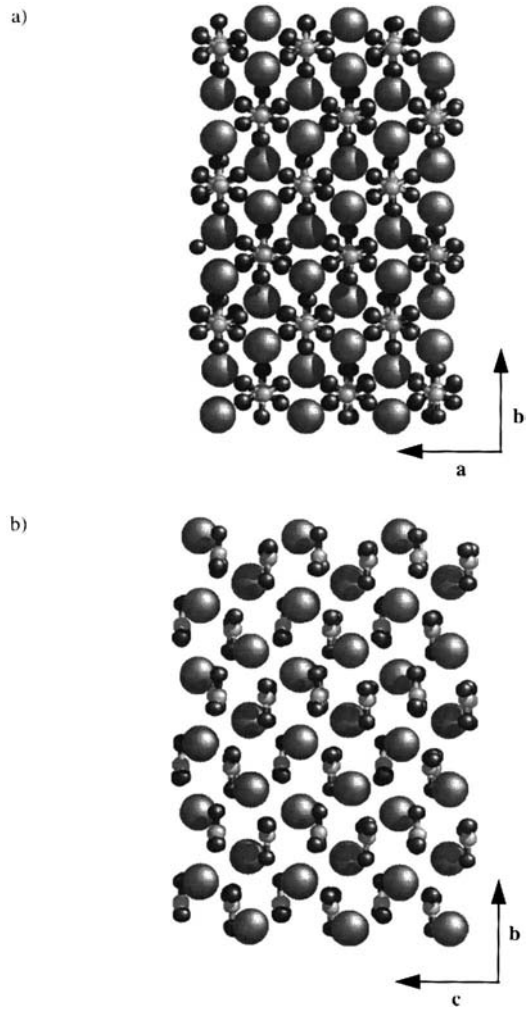

FIGURE 5 The final configuration of the constant volume simulation for aragonite. The labels (a) and (b) denote projections along the *c* and *a* axes respectively. The simulation was carried out at 298 K and a density of 2.944 g cm^{-3}. Other details are as for Figs. 2 and 3.

aragonite, the final system configurations are shown along the *c* and *a* axes of the simulation cell. Again there is apparently very little rearrangement of the structure after the constant volume simulation, when a comparison is made with Fig. 3.

An analysis of the pair radial distribution functions was made, and key atom pair separations were compared with those obtained from X-ray diffraction [13,14]. Figs. 6–11 show respectively the pair radial distribution functions for

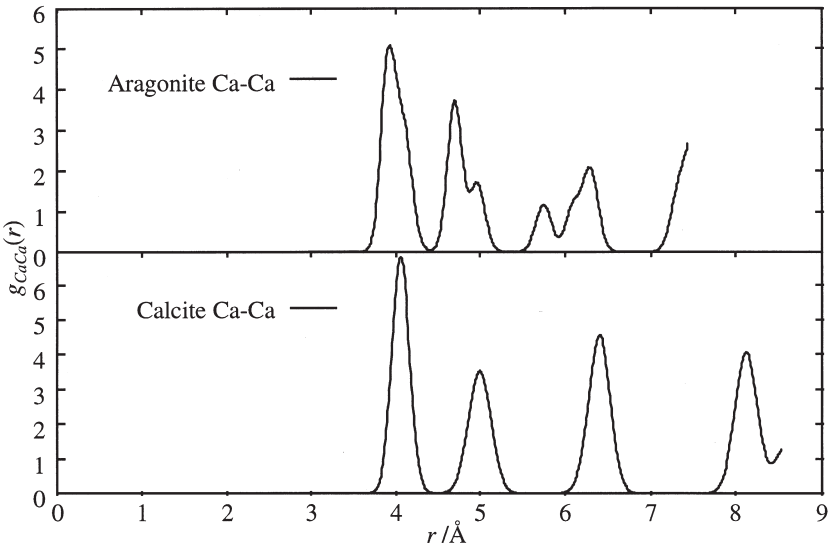

FIGURE 6 The calcium–calcium pair distribution function for constant volume simulations of aragonite and calcite. All simulations were carried out at 298 K, while the calcite system density was 2.71 g cm^{-3} and the aragonite system density was 2.944 g cm^{-3}.

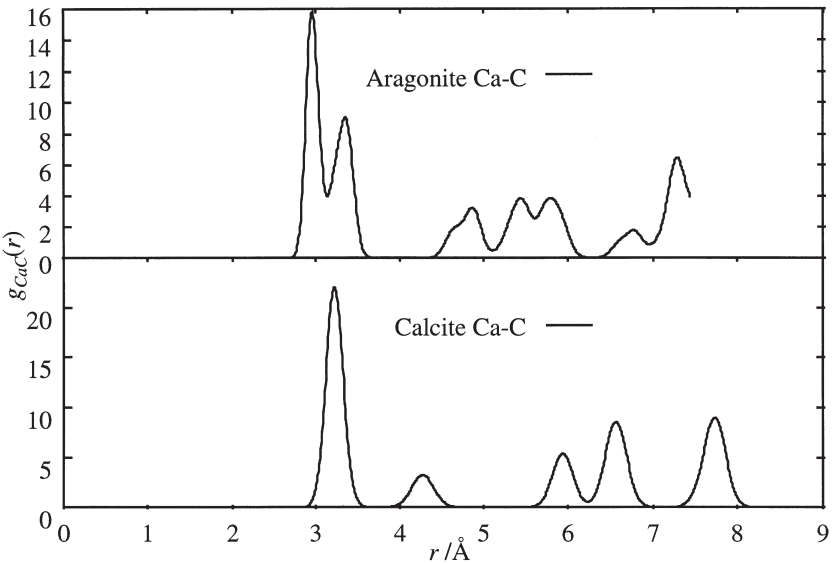

FIGURE 7 As for Fig. 6, except that the calcium–carbon pair distribution functions are shown.

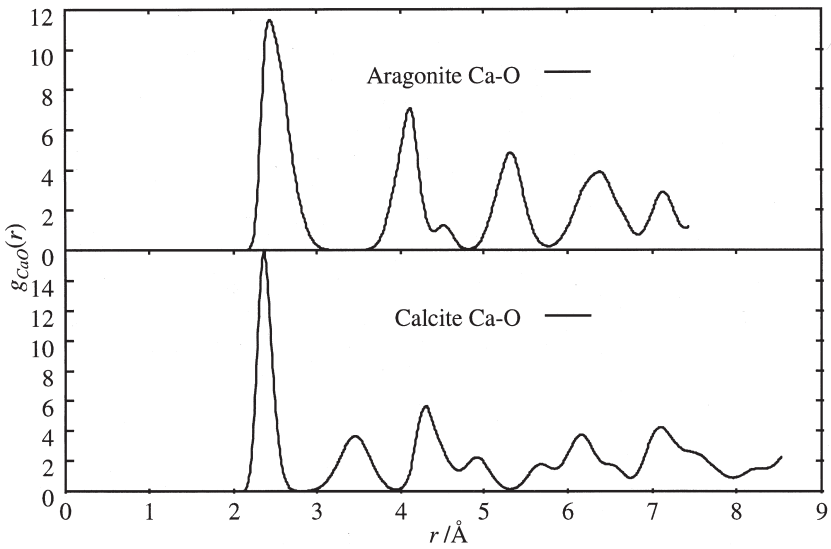

FIGURE 8 As for Fig. 6, except that the calcium–oxygen pair distribution functions are shown.

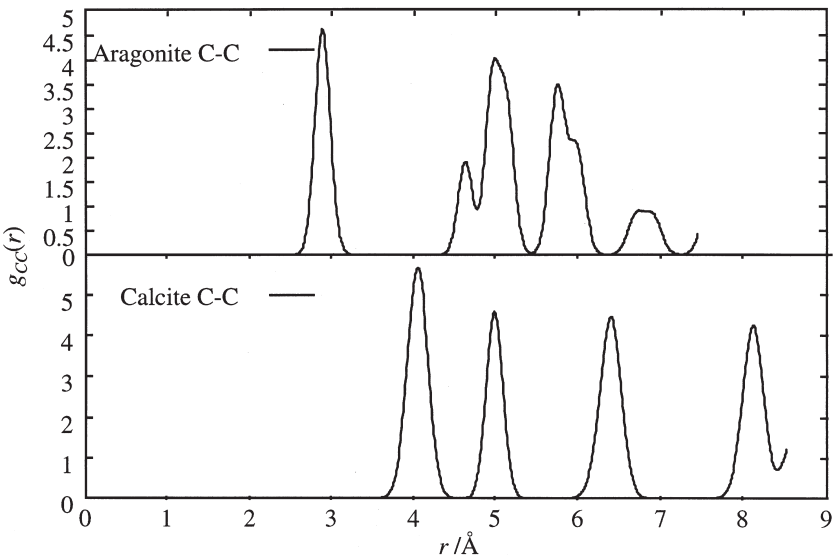

FIGURE 9 As for Fig. 6, except that the carbon–carbon pair distribution functions are shown.

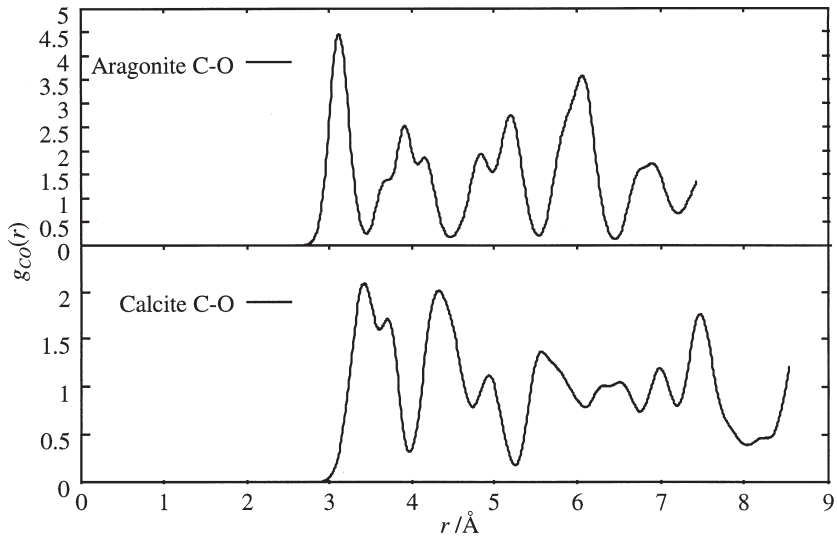

FIGURE 10 As for Fig. 6, except that the carbon–oxygen pair distribution functions are shown.

calcium–calcium, calcium–carbon, calcium–oxygen, carbon–carbon, carbon–oxygen and oxygen–oxygen separations. These pair distribution functions, PDFs, are consistent with the principal co-ordination distances taken from the experimental crystalline structures. Key atom–atom separations from the calcite and aragonite PDFs are compared with the X-ray-derived experimental values in Table IV [13,14]. The X-ray diffraction produced more discrete atom separations than the constant volume simulations. It appears, therefore, that the model showed greater thermal broadening of the peaks than in the experiment data, with coalescence of closely separated peaks into one. In order to compare "like with like", the experimental interatomic distances that were within 0.2 Å were averaged into a single point value. There is a good correlation between the main features of the pair distribution functions below 5 Å calculated from the X-ray crystallographic data and the constant volume simulations of calcite and aragonite.

The agreement between experimental and simulated pair distribution functions would suggest that the force-field reproduces the structural features of calcite and aragonite when using constant volume simulations. However, the constant volume/shape constraints may have had the effect of stabilising metastable structures. Constant stress simulations where carried out to test this hypothesis. In these simulations the hydrostatic pressure of the system was fixed but the cell volume and shape were allowed to vary.

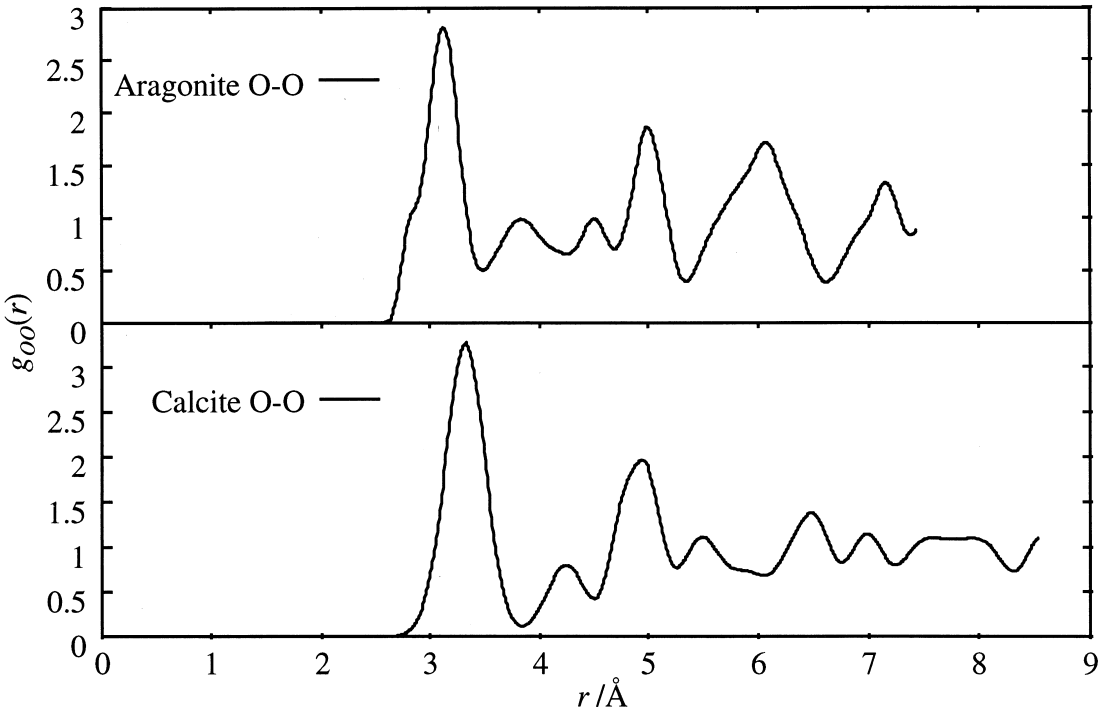

FIGURE 11 As for Fig. 6, except that the oxygen–oxygen pair distribution functions are shown.

TABLE IV Comparison of the species-resolved characteristic radial separations determined from X-ray diffraction (XRD) data [13,14] and molecular dynamics simulations for calcite and aragonite. Data is shown up to distances of 5.0 Å. All simulations were carried out at 298 K. The calcite system density was 2.71 g cm^{-3} and the aragonite system density was 2.944 g cm^{-3}

Atoms i–j	r_{ij} (Å)			
	Calcite, XRD	Calcite, simulation	Aragonite, XRD	Aragonite, simulation
Ca–Ca	4.019	4.053	3.982	3.920
	4.960	4.991	4.692	4.685
			4.960	4.950
Ca–C	3.214	3.209	2.920	2.945
	4.176	4.266	3.329	3.340
	4.960		4.025	
			4.558	
			4.807	4.851
Ca–O	2.360	2.372	2.515	2.433
	3.465	3.465	4.068	4.107
	4.332	4.300	4.480	4.516
	4.871	4.906		
C–C	4.019	4.045	2.8756	2.872
	4.960	4.991	4.642	4.627
			4.949	4.977
C–O	3.400	3.405	3.191	3.117
	3.685	3.702	3.680	3.713
	4.214	4.300	3.993	3.914
	4.461	4.325		4.159
	4.903	4.925	4.801	4.843
O–O	3.213	3.320	3.095	3.120
	3.420		3.599	
	4.224	4.240	3.978	3.824
	4.749		4.308	
	4.946	4.925	4.517	4.513
			4.628	
			4.880	
			4.960	4.990

Constant Stress Simulations

Constant stress simulations were performed on aragonite and calcite. The system was once again evolved from the same crystal structures used in the constant volume simulations, and allowed to equilibrate to ambient temperature and pressure (298 K and 1 bar). The system was considered to have equilibrated when the volume of the simulation dimensions and shape had oscillated about steady values.

Fig. 12 shows the final system configuration of the constant stress simulation performed on model calcite. Comparing this with the starting configuration, given in Fig. 2, it is evident that the calcite structure is not greatly altered by relaxation in the simulation constraints. The final and initial configurations of

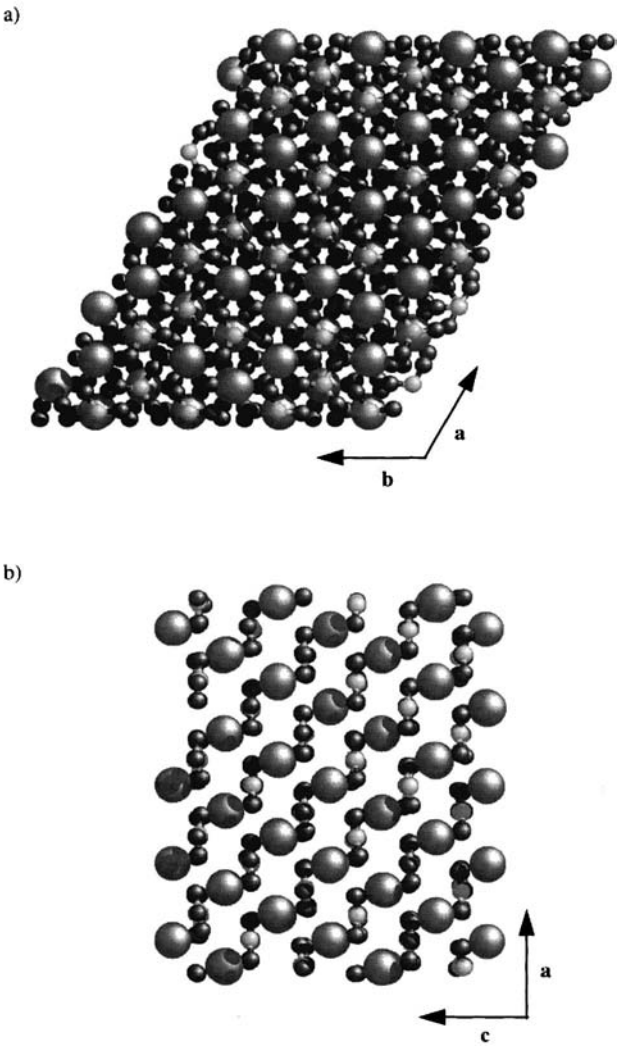

FIGURE 12 The final configuration of the constant stress simulation for calcite: (a) and (b) denote projections along the *c* and *b* axes, respectively. The simulation was carried out at 1 bar pressure and 298 K.

aragonite (see Figs. 13 and 3, respectively) do show some differences. The equilibrated structure from the constant stress simulation indicate that the carbonate ions had rotated through an angle of ca. 60°, although the calcium and carbon centre-of-mass positions did not change appreciably.

The differences in the simulation outcomes can be associated with differences in the carbonate anion geometries between the calcite and aragonite natural

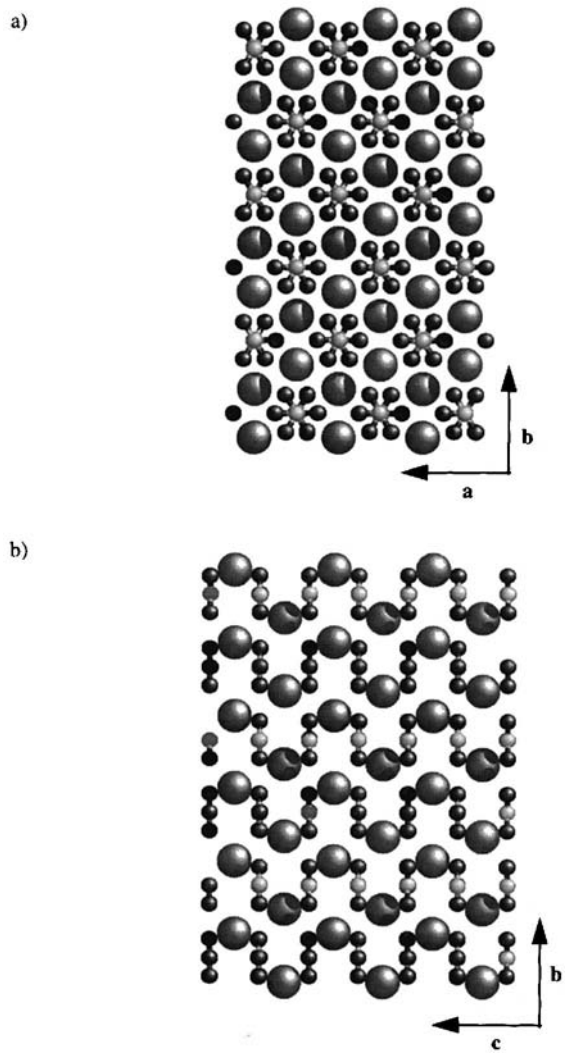

FIGURE 13 The final configuration of the constant stress simulation for aragonite. The labels (a) and (b) denote projections along the *c* and *a* axes respectively. The atom colour coding is the same as for Fig. 2.

crystalline forms. The carbonate in calcite is highly symmetrical, with three equal carbon–oxygen bond lengths of 1.283 Å, three equal bond angles of 120° and a planar arrangement of the carbon and oxygen atoms. The carbonate ion in aragonite, however, has one carbon–oxygen bond length of 1.288 Å and two bond lengths of 1.283 Å. There is one bond angle of 120.1° and two bond angles

of 119.6°. The aragonite carbonate also forms a slightly pyramidal structure with an improper dihedral angle of ca. 184°. The subtle differences in the carbonate geometry in the two forms of calcium carbonate suggest that the force field on the carbonate ion in the aragonite structure is stronger and more anisotropic than in the calcite form, which proves a more severe test of the force-field. Therefore under constant stress conditions the simulation cell is more susceptible to relaxation into a different crystallographic form. It is perhaps not surprising that the force-field produces more satisfactory results for calcite, as it was parameterised for this crystallographic form. Table V compares the unit cell distances obtained from X-ray diffraction (XRD) and the constant stress simulations for calcite and aragonite. The equilibrium unit cell parameters of calcite calculated from the constant stress simulation show a close agreement with the X-ray crystallographic values. Aragonite, however, shows greater differences in the unit cell dimensions. All three lengths, a, b and c were longer so that the density was lower, in fact quite close to the calcite, suggesting that the aragonite phase is tending toward this structure in an attempt to relieve stress on the system.

Table VI compares the component internal energies from the constant volume and constant stress simulations. Considering the calcite system energies, there is very little difference between the total energy of the constant volume and constant stress simulations. The constant volume simulation shows a greater Coulombic and repulsive energy, both of which are reduced in magnitude in the constant stress simulations. This "relaxation" is accompanied by an increase in the bond stretch energy, accompanying the slight increase in the volume of the simulation cell and resulting greater separation of the ions. The bond angle and out-of-plane energies do not change as appreciably between the constant volume

TABLE V Experimental and simulated values for the unit cell parameters and the density of calcite and aragonite [13,14]. The unit cell side lengths are a, b and c while α, β and γ are the internal angles of the unit cell. Constant stress simulations were performed at ambient temperature and pressure.

	Calcite		Aragonite	
	XRD	Constant stress (NσT)	XRD	Constant stress (NσT)
a (Å)	4.990	4.976	4.960	4.987
b (Å)	4.990	4.978	7.964	8.637
c (Å)	17.061	17.449	5.738	5.869
α (°)	90.00	90.01	90.00	90.00
β (°)	90.00	89.98	90.00	90.00
γ (°)	120.00	119.98	90.00	90.00
V_{cell} (Å^3)	367.914	374.518	226.659	252.810
ρ (g cm^{-3})	2.710	2.663	2.944	2.641

TABLE VI System energy components for the constant volume and stress simulations performed on calcite and aragonite. The table shows the coulombic interaction energy, $U_{\text{Coulombic}}$, Born–Mayer repulsive energy, $U_{\text{Born-Meyer}}$, bond stretch energy, $U_{\text{Bond-stretch}}$, bond angle energy, $U_{\text{Bond-angle}}$, out-of-plane energy, $U_{\text{Out-of-plane}}$, kinetic energy, U_{Kinetic}, and total system energy U_{Total}. The constant volume simulations were performed at 298 K and system densities of 2.71 and 2.944 g cm^{-3} for calcite and aragonite respectively. Constant stress simulations were performed at 298 K and 1 bar pressure

	Calcite		Aragonite	
	Constant volume (NVT)	Constant stress (NσT)	Constant volume (NVT)	Constant stress (NσT)
$U_{\text{Coulombic}}$ (kJ mol^{-1})	−1068.8	−1063.8	−1063.0	−1066.5
$U_{\text{Born-Meyer}}$ (kJ mol^{-1})	101.5	95.0	92.8	90.9
$U_{\text{Bond-stretch}}$ (kJ mol^{-1})	2.6	4.3	7.2	8.1
$U_{\text{Bond-angle}}$ (kJ mol^{-1})	1.3	1.4	1.5	1.6
$U_{\text{Out-of-plane}}$ (kJ mol^{-1})	0.9	0.6	0.7	0.0
U_{Kinetic} (kJ mol^{-1})	18.5	18.5	18.4	18.4
U_{Total} (kJ mol^{-1})	−944.1	−944.0	−942.3	−947.4

and constant stress cases, suggesting the flat equilateral carbonate geometry is the same in both types of simulation.

Turning to the aragonite simulations, the total energy of the system decreases a little on removing system volume and shape constraints. There is a significant decrease in the density which causes some decrease in the total energy. Another difference is the out-of-plane energy which at constant stress relaxes essentially to zero, as the carbonate ions can adopt a more planar shape. The constant volume simulation exhibits a slight distortion from planar carbonate geometry. Since the potential was developed for the planar carbonate ion found in calcite, the constant volume aragonite simulation gave a non-zero out-of-plane energy as the carbonate anion was held in a pyramidal conformation by the crystal structure at constant volume. The constant stress conditions provided some relaxation pathways from the initial crystal structure, so that the carbonate ions could become more planar, reducing the out-of-plane potential energy in the process.

In the next section we discuss the results of simulations carried out on the calcium carbonate nano-particles.

Nanoparticle Simulations

Molecular dynamics simulations were carried out to explore the geometry and structure of the particles constructed from the various surfactant molecules. One of the most important tasks was to devise a particle generation procedure that introduced minimal bias into the internal core structure of the particle. Our previous simulations revealed that, once formed, the surfactant molecules were essentially "locked" into place on the surface of the particle by the strong Coulombic forces originating from the inorganic core material [2,4–6], which incidentally goes some way to explain their stability at engine oil temperatures. It was therefore important to *gradually* "condense" the various components in stages from a low density initial state; as once formed there was little likelihood of further significant relaxation and equilibration. After some trial and error we converged on the following method, using elements of two previous works in this area [2,3]. A near-spherical calcium carbonate core containing the desired number of species was "extracted" from a model calcite crystalline lattice. Simulations at a high temperature (ca. 1000 K) were performed to reduce the crystalline order. After "quenching" down to 298 K, surfactant molecules were then deployed at random positions equidistant from the core, with surfactant oxygen atoms typically ca. 2 Å from the mineral surface. The surfactants were aligned radially towards the centre of mass of the core, with alkyl tail groups pointing "outward". The centre of mass of each of the molecules in the system

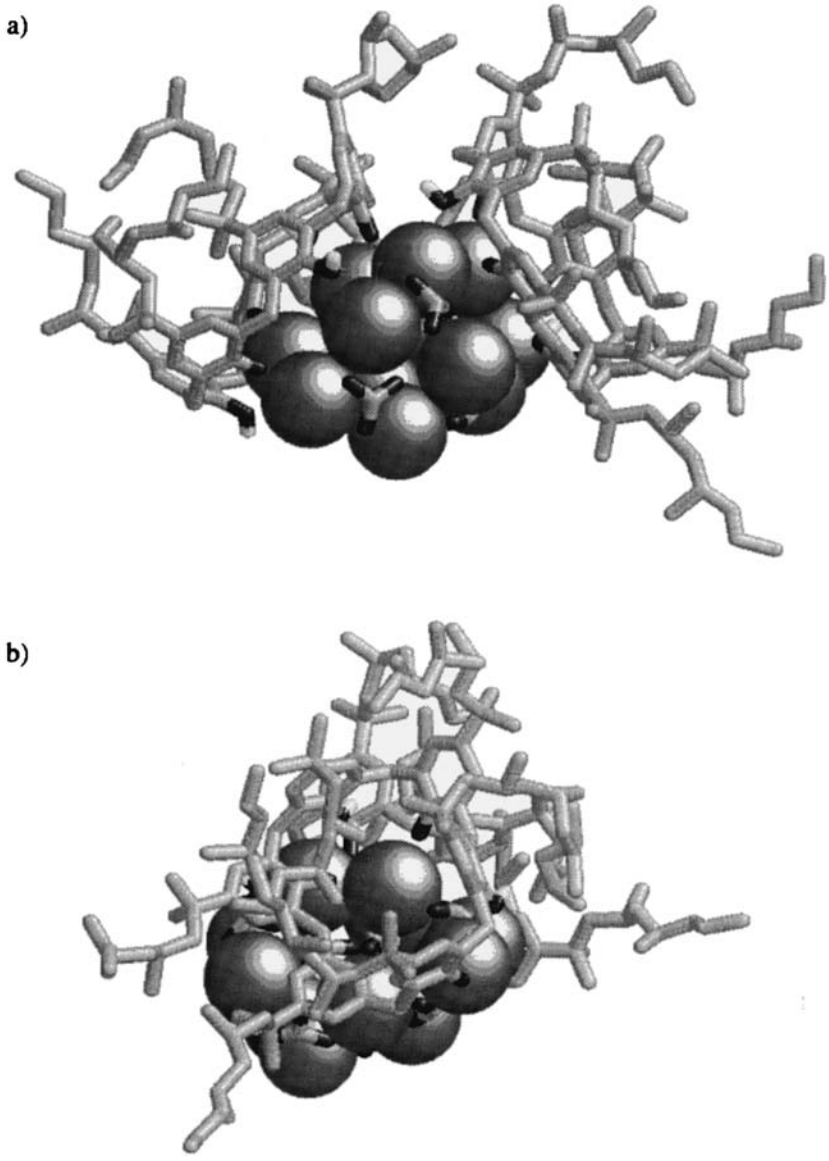

FIGURE 14 (a) Side and (b) end projections of the final system configuration of two calix[6]arate nanoparticles using attractive alkyl tail groups. The end projection is directed through the centre of the macrocyclic calixarates. Space filling representations for the calcium ions and stick representations for the other species are used.

was then scaled by a factor of three so that the structure had a much lower density than that which would stabilise the crystal. Each molecule was then given an initial velocity towards the centre of mass of the core, and the system was allowed to equilibrate at 500 K. The final structure was then allowed to equilibrate at a temperature of 298 K for 500–1000 ps before a final simulation of a further 500ps was carried out to collect data for presentation purposes.

The unified atom force-field, AMBER, of Kollman *et al*. [16,17] was used for the organic fragment interactions. The partial charges on the atoms in the surfactant headgroups were obtained from *ab initio* calculations [18]. The "production" simulations were carried out in a vacuum (without periodic boundary conditions) and at a constant temperature of 298 K. The Coulombic interactions were not truncated, while the non-bonded Lennard–Jones interactions were truncated at 2.8 σ_{max}, where σ_{max} was the largest Lennard–Jones diameter in the system. A time step of 1 fs was used in these calculations.

A series of model overbased detergent systems based on a 250 TBN phenate reference system of 10 calcium carbonate and 6 calcium phenate molecules was simulated. Some preliminary results have been published elsewhere [5,6] and so we only show one example of an isolated particle in Fig. 14 which is based on one with two calix[6]arate rings surfactants. The overall picture that can be derived from a series of simulations with a range of surfactant types is that the calcium carbonate core is covered with strongly bound charged surfactant groups. The deprotonated surfactant head-groups bind strongly to the calcium ions embedded within the surface of the core. In all cases, the structure of the core is amorphous showing no sign of crystal-like order, as may be seen in Fig. 15 which gives the pair radial distribution function between the calcium ions and the carbonate anion oxygen atoms. The short-range order seen for four choices of the surfactant is reminiscent of a simple liquid or glass. It is possible that the simulations were not carried out for long enough to have observed the formation of local domains of crystal-like order. Although, we carried out many tens of such simulations and did not once observe any such local "crystallinity". The relatively large surface to volume ratio of the cores presumably affects the relative stability of the amorphous vs. crystalline forms, in favour of the former.

CONCLUSIONS

In this report we have carried out MD simulations of crystalline calcium carbonate in the calcite and aragonite forms using a parameterised force-field.

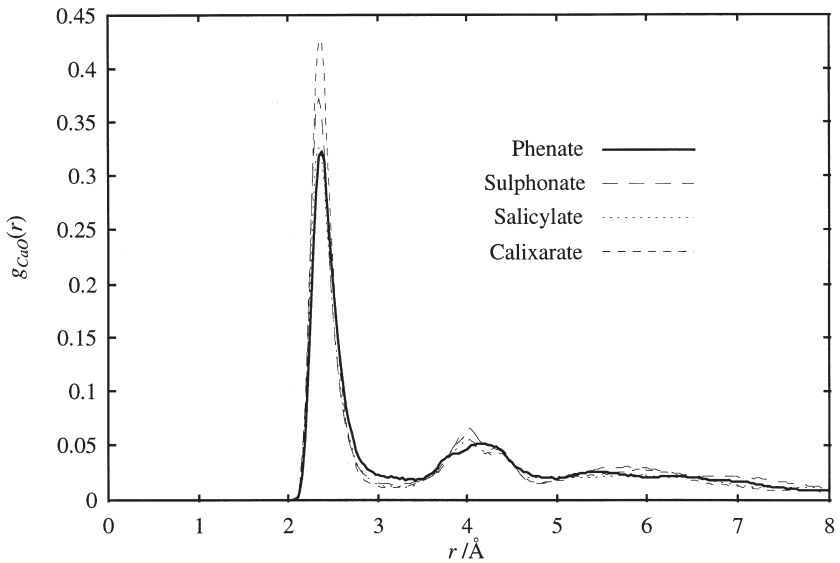

FIGURE 15 The calcium–oxygen (carbonate) pair radial distribution functions for phenate, sulphonate, salicylate and calixarate overbased detergent systems.

The forms adopted accounts reasonably well for these structures, although under unconstrained (constant stress) conditions some distortion of the aragonite structure was noticed. The microstructure of the nanoparticles, in which the calcium carbonate forms the inner core of a core-shell arrangement, appears to be quite different, and amorphous.

Acknowledgements

CAB thanks Adibis Ltd for the provision of a research studentship.

References

[1] Mann, S. and Walsh, D. (1996) "Feigning nature's sculptures", *Chem. In Britain* **32**, 31.
[2] Griffiths, J.A. and Heyes, D.M. (1996) "Atomistic simulation of overbased detergent inverse micelles", *Langmuir* **12**, 2418.
[3] Tobias, D.J. and Klein, M.L. (1996) "Molecular dynamics simulations of a calcium carbonate/calcium sulfonate reverse micelle", *J. Phys. Chem.* **100**, 6637.
[4] Griffiths, J.A., Bolton, R., Heyes, D.M., Clint, J.H. and Taylor, S.E. (1995) "Physico–chemical characterisation of oil-soluble overbased phenate detergents", *J. Chem. Soc. Faraday Trans.* **91**, 687.

[5] Bearchell, C.A., Edgar, J.A., Heyes, D.M. and Taylor, S.E. (1999) "Dielectric spectroscopic and molecular simulation evidence for aggregation of surfactant-stabilized calcium carbonate nanocolloids in organic media", *J. Coll. & Interf. Sci.* **210**, 231.
[6] Bearchell, C.A., Danks, T.N., Heyes, D.M., Moreton, D.J. and Taylor, S.E. (2000) "Experimental and molecular modelling studies of overbased detergent particles", *Phys. Chem. Chem. Phys.* **2**, 5197.
[7] Galsworthy, J., Hammond, S. and Hone, D. (2000) "Oil-soluble colloidal additives", *Current Opinion in Coll. & Interface Sci.* **5**, 274.
[8] Habasaki, J. (1990) "Molecular simulation of molten Li_2CO_3 and Na_2CO_3", *Mol. Phys.* **69**, 115.
[9] Tissen, J.T.W.M. and Janssen, G.J.M. (1990) "Molecular dynamics simulation of molten alkali carbonates", *Mol. Phys.* **71**, 413.
[10] Tissen, J.T.W.M., Janssen, G.J.M. and van der Eerden, J.P. (1994) "Molecular dynamics simulation of binary mixtures of molten alkali carbonates", *Mol. Phys.* **82**, 101.
[11] Genge, M.J., Price, G.D. and Jones, A.P. (1995) "Molecular dynamics simulations of $CaCO_3$ melts to mantle pressures and temperatures—implications for carbonatite magmas", *Earth & Plan. Sci. Lett.* **131**, 225.
[12] Dove, M.T., Winkler, B., Harris, L.M.J. and Salje, E.K.H. (1992) "A new interatomic potential model for calcite—applications to lattice dynamics studies, phase transition, and isotope fractionation", *American Minerologist* **1992**, 77.
[13] Effenberger, H., Mereiter, K. and Zemann, J. (1981) "Crystal structure refinements of magnesite and calcite", *Z. Kristallogr.* **156**, 233.
[14] Dickens, B. and Bowen, J.S. (1971), *J. Res. Nat. B. Stand.* **75A**, 27.
[15] Allen, M.P. and Tildesley, D.J. (1987) Computer Simulation of Liquids (Oxford Science Publications, Oxford).
[16] Weiner, S.J., Kollman, P.A., Case, D.A., Singh, U.C., Ghio, C., Alagona, Jr, G., Profeta, S. and Weiner, P. (1984) "A new force-field for molecular mechanical simulation of nucleic acids and proteins", *J. Am. Chem. Soc.* **106**, 765.
[17] Weiner, S.J., Kollman, P.A., Nguyen, D.T. and Case, D.A. (1986) "An all atom force field for simulations of proteins and nucleic acids", *J. Comp. Chem.* **7**, 230.
[18] Bearchell, C.A. (1999) "Experimental and Computational Studies of overbased detergents". PhD Thesis, University of Surrey.